Hindawi
Mathematical Problems in Engineering
Volume 2019, Article ID 1845056, 12 pages
https://doi.org/10.1155/2019/1845056

Research Article

Optimization of Factors Affecting Vibration Characteristics of Unbalance Response for Machine Motorized Spindle Using Response Surface Method

Elhaj A. I. Ahmed[1,2] **and Li Shusen**[1]

[1]*College of Mechanical and Electrical Engineering, Northeast Forestry University, Harbin 150040, China*
[2]*Department of Mechanical Engineering, Faculty of Engineering Science, University of Nyala, Nyala, P.O. Box 155, Sudan*

Correspondence should be addressed to Li Shusen; lishusenzp@126.com

Received 4 October 2018; Revised 20 December 2018; Accepted 22 January 2019; Published 10 February 2019

Academic Editor: Mohammed Nouari

In this study, the response surface (RS) method and forced rotordynamic analyses together with Finite-Element-Analysis (FEA) have been established to optimize the factors affecting the vibration characteristics. The spindle specification, bearings locations, cutting force, and motor-rotor unbalance mass are proposed to represent the design factors and then they are utilized to develop Machine Motorized Spindle (MMS). The FEA-based Design of Experiment (DOE) is adopted to simulate the output responses with the input factors, wherein these DOE design points are used to carry out the RS models to visualize more obvious factors affecting the dynamic characteristics of MMS. The sensitivities of these factors and their contributions to the vibration of imbalance response have been evaluated by using the RS models. The simulation results show that the motor-rotor shaft inner diameter, the distance of the back bearing location, and the rotating unbalance-mass are highly sensitive to the vibration characteristics compared to the other factors. It is found that more than two-fifths of total vibration response amplitude has been conducted by induced rotating imbalance mass. The results also showed that the proposed factors optimization method is practicable and effective in improving the vibration response characteristics.

1. Introduction

In the machined component, the machining accuracy is most critical and is related to several factors, wherein these factors include thermal error, positioning error, tool-holder and rotating unbalance force induced error, and motion error [1]. To improve the accuracy of machining, these aforementioned errors have been significantly recognized and rewarded by the certain situation of art method, for instance, the machine-tool movement errors [2], thermal induced deformation [3], and deflection due to the cutting tool in small milling [4]. Optimization of parameters influencing the vibration characteristics of spindle under rotating unbalance force induced is the research foundation for lively balancing control that is more important in vibration monitoring and control. Because of complex structures of MMS, the optimization of parameters affecting its dynamic characteristics due to motor-rotor unbalance induced is much difficult [5]. Recently, considerable researches have been carried out to improve the vibration response characteristics of MMS. The effects of design variables or operation parameters on system dynamics response have been covered with the inclusive variety of researches [6–12]. These previous researches were focused on improving the dynamic performances of high-speed (HS) motorized spindle through optimizing the design factors. The effect of operating parameters on the system dynamics response is also enclosed by several kinds of researches [13–19]; they focused on improving the machining parameters that affect the surface roughness of different materials machined on various CNC machines. A significant effort has been exerted on the design optimization of a motorized-spindle-bearing system. Lee et al. [20] proposed a design optimization method to reduce the mass of a flexible rotor supported in ball bearings via rotational velocities and

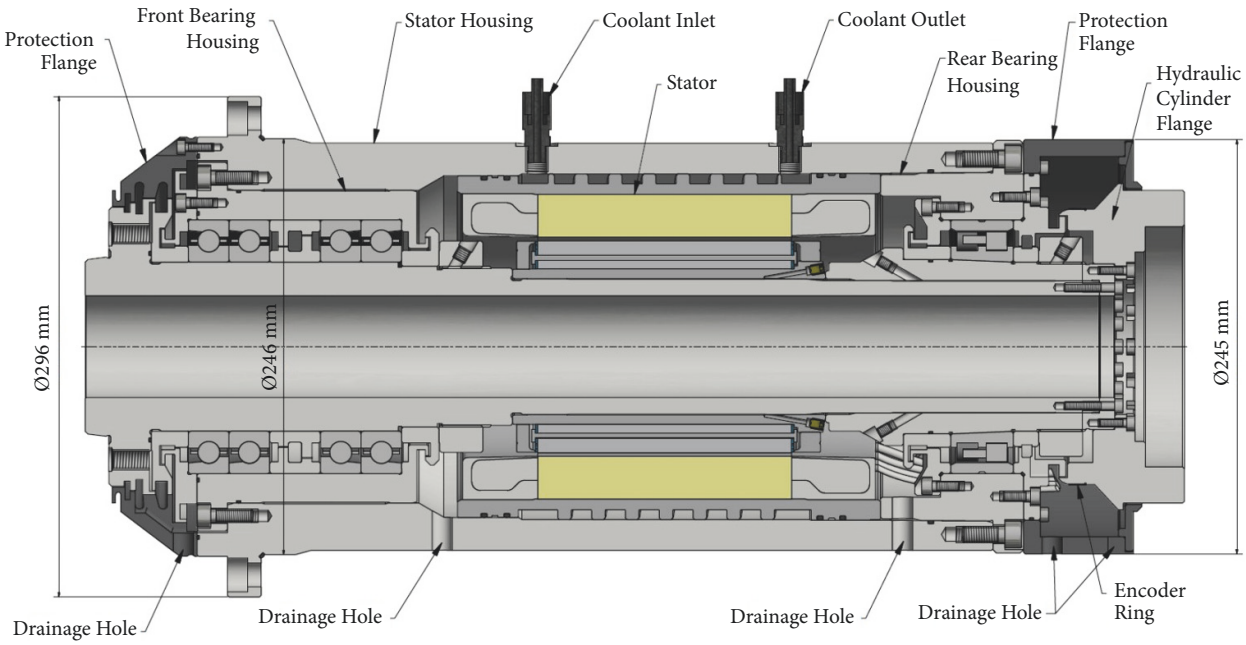

Figure 1: The Section view of the MMS.

load reliant on stiffness characteristics in constraints of the bearing fatigue life and system eigenvalues. Lin Y.-H. and Lin S.-C. [21] proposed the finite-element-method to develop the reduced-weight design of a spindle supported by oil-lubricant bearing under a frequency constraint using a successive quadratic programming method. Lin C.-W. [22] developed a mathematical model for an optimization problem to reduce the total costs of the tolerance and a predictable value of the dissipated quality, under definite constraints. They proposed an optimization technique that integrated the Monte-Carlo Simulation and genetic-algorithm to simultaneously explore the optimal design vectors and tolerance of bearings. Lin C.-W. [23] also applied Taguchi technique to recognize the optimal values of design vectors for a robust HS spindle system with respect to the signal/noise ratio of system First-Mode-Natural-Frequency (FMNF) under gyroscopic moment effect. Most of these studies were focused on improving the dynamic characteristics, through simultaneously minimizing the material used in the structure and maximizing the FMNF of different spindle-systems. However, the studies on optimization of factors affecting the vibration response characteristics of MMS under rotating unbalance force effects due to its complex dynamic model has been relatively lacking. Usually, the designer mostly focused on unforced vibration design optimization. However, the influence of the gyroscopic moments and motor-rotor imbalance forces on the dynamic response are slightly disregarded. This system design manner is unsatisfactory for balancing and control of the machine vibration. In HS machining, the extra loads created by rotating elements may well cause a greatest influence on the quality of the machined component. For instance, due to HS machining, the gyroscopic moment effects and rotating unbalance forces will generate more vibration for the MMS, which directly affects the dynamic performances of MMS. Therefore, to precisely predict the actual performance of MMS it is necessary to conduct the vibration design under rotating elements forces induced. In the present work, optimization of the factors affecting vibration characteristics under rotating unbalance force effect is presented. The RS method and forced rotordynamic analyses along with FEA are used to determine the optimal combinations of the factors that improve the vibration behaviors of MMS. The spindle specifications, bearings locations, cutting force, and motor-rotor unbalance mass are proposed to represent the design factors, and then they are utilized to develop MMS. The Central-Composed-Design (CCD) and Box-Behnken Design (BBD) approaches, due to their efficiency in providing considerable data in a least number of required statistical experiments, are adopted to generate the DOE, wherein these DOE design points data then are used to build the RS models. To visualize more obvious design factors affecting the dynamic characteristics of MMS, the RS evaluation is carried out in detail. The sensitivities of design factor on the vibration response and the optimization of their levels are covered by using these RS models. Finally, direct real solution of the finite element model (FEM) and literature results are used to examine the quality of the RS model considered.

2. Motorized Spindle System Specifications

Figure 1 shows the section view of lathe motorized spindle, which was established to hold motorized spindle rather than conventional-pulley drive L-series lathe spindle, standard JIS A2-6 [24]. It is designed to withstand maximum 3700N of cutting force and 7000 rpm of machining velocity and pulled by a 16.8kw motor coupled to the shaft with synchronous-motor Type 1FE1093-6WV. The SKF-roller-bearings under

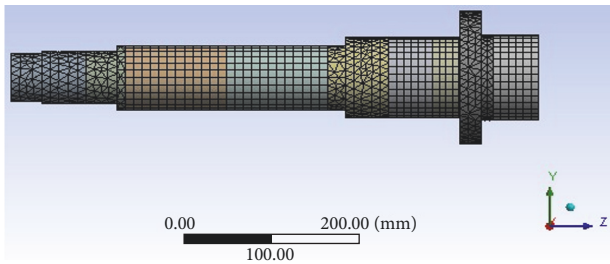

Figure 2: The developed finite element model of MMS with meshing.

the designation of 7220BECBY and NNCF5013CV were presented to support spindle at bearings locations. The MMS shown in Figure 1 is developed as an example case to conduct the FEA-based DOE for RS evaluation. In order to predict the vibration response under all sensational loads, the workpieces holder (chuck standard B6151sc) is also considered in the FEM.

2.1. Finite Element Model-Based Experimental Design. The MMS withstanding various forces under operation condition is utilized in this work, wherein these forces include the rotating unbalance force transmitted to the spindle via the electric motor and the cutting-load applied at the spindle-nose. Based on ANSYS SpaceClaim, the 3D FEM for MMS is established. In order to simplify the simulation process, all the induced masses for the chuck and motor-rotor are modeled as a point mass (MASS21 element) with remote point type connection under inertia load effects. The bearings are modeled by using 2D elastic spring-damper-element (COMBI214) by ground-to-body type connection. The bearings stiffness is estimated according to the bearing specifications, which is 4x10E5N/mm for front bearing, and is 3.5x10E6N/mm for the back bearing. The structural damping ratio is 0.05. The bearing stiffness is adjusted as an invariable value since the effect of a load of bearing and rotational speed on the stiffness of bearing is disregarded. To constrain degree of freedom on axial direction, the displacement constraint is added to both front bearings positions and back bearing position. Automatic mesh division method is used to mesh the entire structural model of MMS. The entire spindle model has been meshed by considering the magnitude and accuracy of the design; the selected size of the mesh unit was 10 mm; hence the FEM meshing is shown in Figure 2. The material used in this study is structural steel (E = 210GPa, ρ = 7850kg\m^3 and υ = 0.3).

2.2. Unbalance Response Analysis. To analyze the vibration of unbalance response, the motor-rotor unbalance force induced and cutting force are used for exciting the FEM. The unbalance force varied occasionally according to the sinusoidal rule as follows [5]:

$$\mathrm{F}(t) = Mr\omega^2 \sin \omega t = \vec{\mathrm{X}}\omega^2 \sin \omega t \tag{1}$$

where M, r, ω, and X are represented rotor mass, radius of the rotor, excitation frequency, and amplitude response,

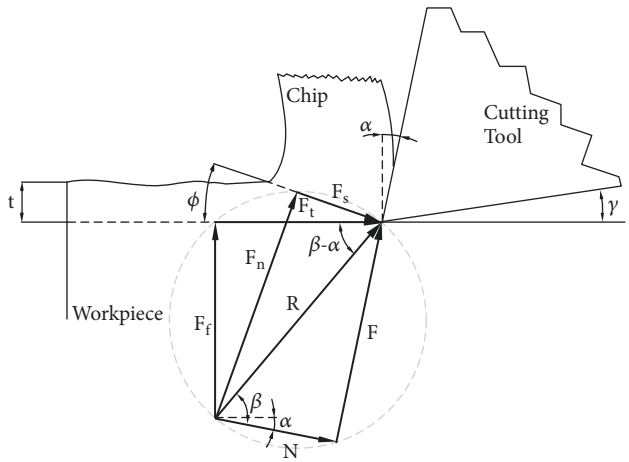

Figure 3: Merchant circle with cutting force diagram.

respectively. In this study, the excitation force is defined by rotor unbalance mass and its radius in ANSYS mechanical environment. To calculate the cutting force we examined the sample case of 200HB AISI 4340 part of steel with a diameter of 110 mm, length of 50 mm, under machining condition of 0.35 mm/rev feed rate, 6 mm depth of cut, and 600 rpm spindle speed. According to this case, the components of the resultant cutting force can be found from the Merchant circle shown in Figure 3, as follows [24]:

$$\begin{aligned} \mathrm{F}_t &= \mathrm{TB}_c\mathrm{N}_s \frac{\cos(\beta - \alpha)}{\sin(\phi)\cos(\phi + \beta - \alpha)} \\ \mathrm{F}_f &= \mathrm{TB}_c\mathrm{N}_s \frac{\sin(\beta - \alpha)}{\sin(\phi)\cos(\phi + \beta - \alpha)} \end{aligned} \tag{2}$$

where T, Bc, and Ns represent chip thickness, the width of the cut in a radial direction, and shear strength of the material, respectively. The tangential force factors and specific cutting can be determined according to [24]. In this study, the vibration responses for the stress, strain, and deformation amplitude at span between bearings were taken as output responses in the evaluation of MMS. The definitions of factors used to control the output responses are defined in detail where their lower and upper levels are shown in Table 1. The forced rotordynamic analyses for the MMS under excitation of cutting force and motor-rotor unbalance mass are established within the excitation frequency range of 60-600Hz, by using the direct integration method.

2.3. Design of Experiment. The DOE is a method originally advanced for prototypical fitting with experimental data, in which the affiliation between the factors, their interactions, and the output response is defined [25]. In RS method, the DOE can be used to fit the simulated response data to mathematical models. The RS method contains the number of DOE types, such as CCDs and BBD in which each type is used to achieve specific functionality. The main difference of BBD from CCDs is three level quadratic designs in which the explored space is represented by $[-1, 0, +1]$. For more

Table 1: The definition of design factors, their lower and upper limits, and the FEM nominal level.

Definition	Design factors	Lower Level	Nominal Level	Upper Level
The inner diameter of spindle shaft at the back bearings location.	Y1 [mm]	40	45	55
The inner diameter of spindle shaft at the motor-rotor location.	Y2 [mm]	40	45	60
The inner diameter of spindle shaft at the front bearings location.	Y3 [mm]	50	54	60
The locations of back bearings set to the back end of the motor rotor.	Y4 [mm]	10	50	70
The locations of first front bearings set to the front end of the motor rotor.	Y5 [mm]	20	50	60
The locations of second front bearings set to the front end of the motor rotor	Y6 [mm]	10	50	60
Cutting Force	Y7 [N]	3330	3700	4000
Rotating Unbalance mass	Y8 [kg]	0	6	10

quality experiment designs, the CCDs and BBD due to their efficiency in providing much data in a nominal number of required statistical experiments have been adopted to run the experiments. These experiments were adjusted according to upper and lower limits of the factors explained in Table 1. The numbers of experimental runs are conducted to find out the responses for stress, strain, and total deformation (TD) at the bearings span, as well as Structural Weight (SW). The Auto-Define (AD) and Face-Cantered (FC) options are used to perform the experiments of CCDs. The experiments are carried out as follows: first, 82 experimental runs for AD-CCD, second, 82 experimental runs for FC-CCD, and, third, 65 experimental runs for BBD. Then, the best results have been obtained after repeating the experiments many times for each approach. In the later sections, the comparison between these experiments designs is carried out to define the most refined RS model.

3. Results and Discussions

After the design space is sampled in DOE, the responses dataset can be obtained through the FEM simulation. To evaluate the sensitivities of factors on the vibration responses, the variation of input with output responses is graphically presented based on genetic-aggregation method. For more refined RS results, the best-fit curve and its verifications are carried out to evaluate the quality of the RS model. The interpolation models that provided continuous variation of the responses with respect to the design factors are used to fit the response surface model. The goodness fit curves for stress (P39), strain (P40), and TD (P41) and their verification are represented in Figure 4. From Figures 4(a), 4(b), and 4(c), it can be shown that the scatter charts presented are normalized for the values of each output response. Among these models, Figure 4(c) is more precise from the view of verification point, and it can be clearly seen in Figure 4(d) after refinement.

As results discussed for the quality of RS, the BBD approach is more significant than CCDs approaches from the view of the best-fit plots and verification points. Thus, the DOE models generated by CCD methods could be omitted from later RS evaluation. The raw BBD design point's data are provided in Table 2, in which the most design points obtained by BBD are described. These BBD design points are used to build RS models for the sensitivities analysis, in addition to the RS optimizer, wherein the RS optimizer draws information from the RS model.

3.1. Sensitivities Analysis. The contributions of the variables on the dynamic response are graphically plotted in Figure 5. It revealed that the higher input percentages show that the corresponding design variable has a stronger effect on the output amplitude of stress P39, strain P40, and TD P41. The factors Y2, Y4, and Y8 have the greatest effect on the output response, whereas the other variables have the smallest influences on the output response. From Figures 5(a), 5(b), and 5(c) it can be seen that the effect of factor Y8 on the vibration amplitude is the first, factor Y4 is the second, and factor Y2 is the third. Among these factors the vibration response conducted by Y8 is the largest when it compared to Y2 and Y4. For example, in Figure 5(a), Y4 and Y8 are more effective parameters for stress response. In Figure 5(b), Y2 and Y8 are more significant parameter for strain response, while in Figure 5(c) their effect on TD response is as follows: Y8, Y4, and Y2, respectively. Thus, the rotating unbalance-mass (Y8) and the motor-rotor shaft inner diameter (Y2) are the vital factors that entirely control the vibration responses for MMS.

In order to obtain the specific contribution of factors of Y4, Y2, and Y8 on the vibration responses, the interpolation models that provided continuous variation of input with output responses are graphically plotted in Figures 6 and 7, respectively. As seen, the effect of each factor on output response at different step points can be observed, and the least output response always yields the optimum dynamic characteristics. Thus, the smallest amount of the output response will define the most favorable level of each factor. Figure 6 shows that the relationship between the output response with Y4 in Figures 6(a) and 6(c) is linear, whereas in Figure 6(b) it is nonlinear. Similarly, it can be shown from Figure 7 that the variation of the output response with Y2 and Y8 is approximately nonlinear, where the vibration response is decreased or elevated with increasing the variable space along their difference limits.

As a result, to enhance an optimum performance of MMS the factors Y2 and Y4 should be kept at maximum potential, while the factor Y8 should be kept as minimum as possible. From the view of RS evaluation, the optimal combinations of the response points observed are as follows: Y1 [47.5mm], Y2 [50mm], Y3 [55mm], Y4 [40mm], Y5 [35mm], Y6 [40mm], Y7 [3665.2N] and Y8 [5kg], stress response [0.108MPa], strain response [2.1E-7mm/mm], and TD response [0.31mm].

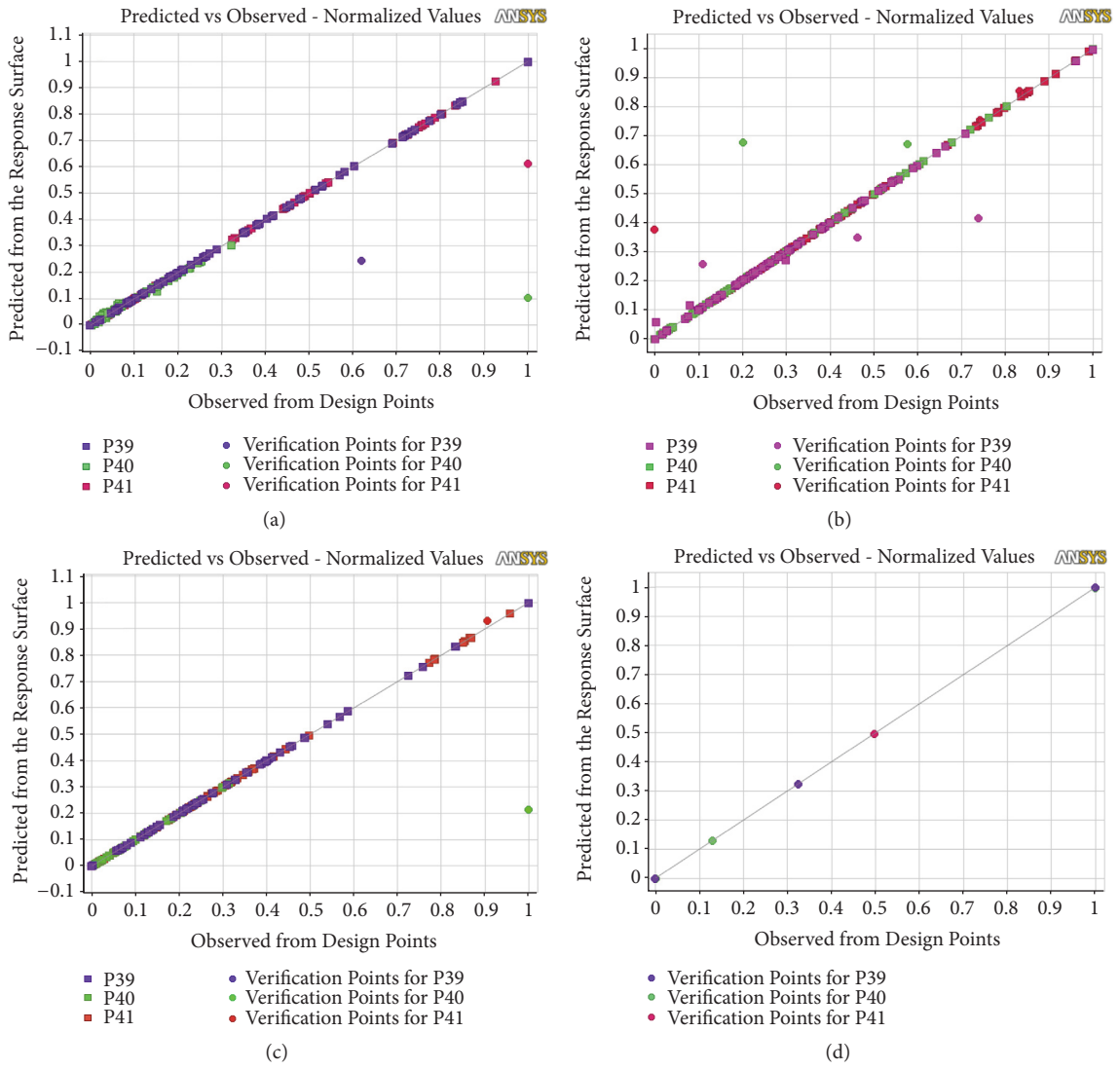

Figure 4: The output response simulated by the RS vs. that observed from the DOE, (a) Auto-Define-CCD, (b) Face-Centred-CCD, (c) BBD, and (d) refined BBD.

3.2. Optimization. To find the optimum combination of variables that improve the dynamic response, the optimization is carried out based on RS evaluations in Section 3.1. The objective function and constraint are defined according to (3), including SW and TD. The two most popular RS optimizations are Multiobjective Genetic Algorithm (MOGA) and screening methods (SM). To obtain more refined results, MOGA and SM have been utilized to increase the numbers of the RS optimization runs. The Direct Optimization (DO) is also conducted to check the quality of RS optimization, since it utilizes a real calculation rather than RS evaluation. The optimization configuration is adjusted to generate 2000 samples initially and 100 samples per iteration and found the optimum candidates point in a maximum of 20 iterations. Each optimization method has suggested three optimum candidate points as summarized in Table 3. From the results shown in Table 3, it is noted that the candidate's points for RS are comparable to real solutions of DO, except minor variation among the results. Based on the criteria of the maximum allowed cutting force, rotating unbalance mass, and minimum SW, the candidates' points highlighted by $*$ in Table 3 are more significant. Thus, these marked candidates' points are suggested to represent the optimal combination of factors that improve the vibration behaviors of MMS. Also, it can be showed that the SW is improved to 19.45% saving; hence not only does the proposed method enhance the design factors, but also the material resource consumed can be reduced.

$$\text{Find } Y = (Y1, Y2, Y3, \ldots, \ldots, Y8) \tag{3}$$

Table 2: The design points of BBD experiments data.

Run	Y1	Y2	Y3	Y4	Y5	Y6	Y7	Y8	Stress [MPa]	Strain [mm\mm]	TD [mm]	SW [kg]
1	47.5	50	55	40	35	40	3665	5	0.10805	2.04E-07	0.315214	17.42614
2	40	50	50	40	35	20	3665	5	0.08361	4.08E-07	0.308941	18.18693
3	55	50	50	40	35	20	3665	5	0.05578	5.19E-07	0.350467	17.44491
4	40	50	60	40	35	20	3665	5	0.1347	1.35E-07	0.307662	17.30887
5	55	50	60	40	35	20	3665	5	0.11597	2.24E-07	0.34802	16.56685
6	40	50	50	40	35	60	3665	5	0.08623	5.08E-07	0.290122	18.18693
7	55	50	50	40	35	60	3665	5	0.03871	4.35E-07	0.321984	17.44491
8	40	50	60	40	35	60	3665	5	0.04787	4.17E-07	0.293676	17.30887
9	55	50	60	40	35	60	3665	5	0.01637	4.26E-07	0.324317	16.56685
10	47.5	40	50	40	10	40	3665	5	0.14505	4.34E-07	0.314232	19.27872
11	47.5	40	60	40	10	40	3665	5	0.0999	2.47E-07	0.315685	18.40066
12	47.5	60	50	40	10	40	3665	5	0.06471	6.89E-07	0.337772	16.09314
13	47.5	60	60	40	10	40	3665	5	0.10354	4.61E-07	0.337358	15.21509
14	47.5	40	50	40	60	40	3665	5	0.14425	4.37E-07	0.290244	19.27872
15	47.5	40	60	40	60	40	3665	5	0.10226	1.96E-07	0.29403	18.40066
16	47.5	60	50	40	60	40	3665	5	0.0559	6.61E-07	0.30426	16.09314
17	47.5	60	60	40	60	40	3665	5	0.10669	3.62E-07	0.304491	15.21509
18	47.5	40	55	10	35	40	3665	0	0.12801	8.31E-07	0.433314	18.85965
19	47.5	60	55	10	35	40	3665	0	0.22891	1.12E-06	0.418388	15.67407
20	47.5	40	55	70	35	40	3665	0	0.05891	4.35E-07	0.227901	18.85965
21	47.5	60	55	70	35	40	3665	0	0.13504	6.92E-07	0.275409	15.67407
22	47.5	40	55	10	35	40	3665	10	0.2121	1.41E-06	0.730907	18.85965
23	47.5	60	55	10	35	40	3665	10	0.3791	1.86E-06	0.708668	15.67407
24	47.5	40	55	70	35	40	3665	10	0.09917	7.54E-07	0.381429	18.85965
25	47.5	60	55	70	35	40	3665	10	0.22209	1.14E-06	0.461991	15.67407
26	47.5	50	55	10	35	20	3330	5	0.18199	1.37E-07	0.394835	17.42614
27	47.5	50	55	70	35	20	3330	5	0.03595	5.71E-07	0.205719	17.42614
28	47.5	50	55	10	35	60	3330	5	0.16095	2.59E-07	0.345363	17.42614
29	47.5	50	55	70	35	60	3330	5	0.01503	3.55E-07	0.195859	17.42614
30	47.5	50	55	10	35	20	4000	5	0.18034	1.39E-07	0.392291	17.42614
31	47.5	50	55	70	35	20	4000	5	0.03717	5.67E-07	0.204992	17.42614
32	47.5	50	55	10	35	60	4000	5	0.15953	2.62E-07	0.342976	17.42614
33	47.5	50	55	70	35	60	4000	5	0.01501	3.56E-07	0.195504	17.42614
34	40	50	55	40	10	20	3665	5	0.10713	4.35E-07	0.317481	17.76786
35	55	50	55	40	10	20	3665	5	0.09067	5.06E-07	0.363253	17.02583
36	40	50	55	40	10	60	3665	5	0.07181	2.56E-07	0.299475	17.76786
37	55	50	55	40	10	60	3665	5	0.04018	1.55E-07	0.332554	17.02583
38	40	50	55	40	60	20	3665	5	0.11663	4.99E-07	0.295696	17.76786
39	55	50	55	40	60	20	3665	5	0.1021	4.73E-07	0.332294	17.02583
40	40	50	55	40	60	60	3665	5	0.07022	3.24E-07	0.275881	17.76786
41	55	50	55	40	60	60	3665	5	0.04082	1.74E-07	0.30406	17.02583
42	47.5	50	50	40	10	40	3665	0	0.17247	5.46E-07	0.39225	17.84521
43	47.5	50	60	40	10	40	3665	0	0.09173	7.49E-07	0.393006	16.96715
44	47.5	50	50	40	60	40	3665	0	0.1656	4.75E-07	0.362988	17.84521
45	47.5	50	60	40	60	40	3665	0	0.09054	8.99E-07	0.366577	16.96715
-	-	-	-	-	-	-	-	-	-	-	-	-
-	-	-	-	-	-	-	-	-	-	-	-	-
61	55	50	55	70	35	40	3330	5	0.06956	2.76E-07	0.211405	17.02583
62	40	50	55	10	35	40	4000	5	0.06667	2.57E-07	0.356704	17.76786

Table 2: Continued.

Run	Y1	Y2	Y3	Y4	Y5	Y6	Y7	Y8	Stress [MPa]	Strain [mm\mm]	TD [mm]	SW [kg]
63	55	50	55	10	35	40	4000	5	0.06236	4.62E-07	0.371103	17.02583
64	40	50	55	70	35	40	4000	5	0.04448	1.82E-07	0.20032	17.76786
65	55	50	55	70	35	40	4000	5	0.06965	2.74E-07	0.210732	17.02583

Table 3: Initial design, optimal candidate points, and real solution or DO.

Design Factors	Initial Design	Response Surface Optimization						DO (SM)
		(MOGA)			(SM)			
		1∗	2	3	1	2	3∗	
Y1 [mm]	45	54.4	54	54.3	50.7	48	52.3	50.7
Y2 [mm]	45	59.9	59.9	59.8	59.2	59.5	56.4	58.4
Y3 [mm]	54	59.9	59.7	59.8	59.5	58.4	51.1	59.4
Y4 [mm]	50	68.4	67.9	68.4	66.7	63.7	68.7	53.4
Y5 [mm]	50	42.2	46.9	42.3	32.5	12.2	59.1	10.9
Y6 [mm]	50	50.3	50	42.5	51.9	20.5	52.9	42.4
Y7 [N]	3700	3937.9	3988.4	3859.8	3546.2	3835.9	3678.4	3302.4
Y8 [kg]	6	5.2	5.3	5.5	3.3	4.7	4.5	0.67
SW [kg]	18	14.5	14.6	14.5	15.1	15.2	15.4	15.4
TD [mm]	0.225	0.22	0.22	0.23	0.23	0.25	0.19	0.086

$$\text{Minimize} \quad \text{SW} = \sum_{k=1}^{N} \rho_k \text{A}_k \text{L}, \ \textit{where}: \rho \textit{ is density}, \ A \textit{ is area}, \ L \textit{ is element length}$$

$$\text{Subjected to} \quad \begin{cases} TD \le 0.26mm & \textit{and } N \textit{ elements number} \\ 40 \le Y1 \le 55, & 40 \le Y2 \le 60 \\ 50 \le Y3 \le 60, & 10 \le Y4 \le 70 \\ 20 \le Y5 \le 60, & 10 \le Y6 \le 60 \\ 3330 \le Y7 \le 4000, & 0 \le Y8 \le 10 \end{cases} \tag{4}$$

The TD found in the proposed approach is relatively high, because the simulated results are conducted in maximum excitation frequency of 600Hz. According to the design criteria of this MMS (167Hz machining speed), the FMNF should be 30% higher than operation frequency [26]. To examine the TD at FMNF (200Hz), the real solution for RS analysis results has been carried out. The solutions are conducted by inserting the optimal design points obtained by MOGA and SM as well as DO into the current design points and then are updated in the FEM. The FEA real solving results for these optimization methods are graphically represented in Figure 8. From Figures 8(a), 8(b), and 8(c), it can be seen that the maximum TD is found in the range from 0.037mm to 0.049mm; hence the optimized FEMs fully met the design requirements [28]. Among these models, the FEM in Figure 8(a) is more significant model that meets the cutting force requirements. Furthermore, the comparison between the FEA and the RS analysis results is carried out in Figure 9, wherein the FEA denotes the initial design, since the RS analysis refers to the design points 1∗ in Table 3. From Figure 9, it is noted that these FRF results obtained are similar, confirming that the design points of BBD are accurately fitted to the RS models.

To check the quality of FEM, the experimentally validated results in [1] and the FEA results in [26, 27] are used to verify this FEM by calculating the dimensionless amplitude. The dimensionless amplitude is known as the ratio of dynamic TD to Static Deformation (SD) under external force. In fact, the SD of the spindle-shaft has been constrained by the theory of the maximum SD; hence it should be less than or equal to 0.0002 of the span between bearings for adequate rigidity [28]. The dynamic TD amplitude is considered at the FMNF. With assuming that SD is constrained by literature, the dimensionless amplitude for optimal FEM and [1, 26, 27] are reported in Table 4. From Table 4 it is noted that there are minor differences among these values due to the difference in material properties, boundary condition, etc. As results discussed, the proposed factors optimization method is feasible and successful in improving the vibration characteristics. Thus, it can be considered as a practical

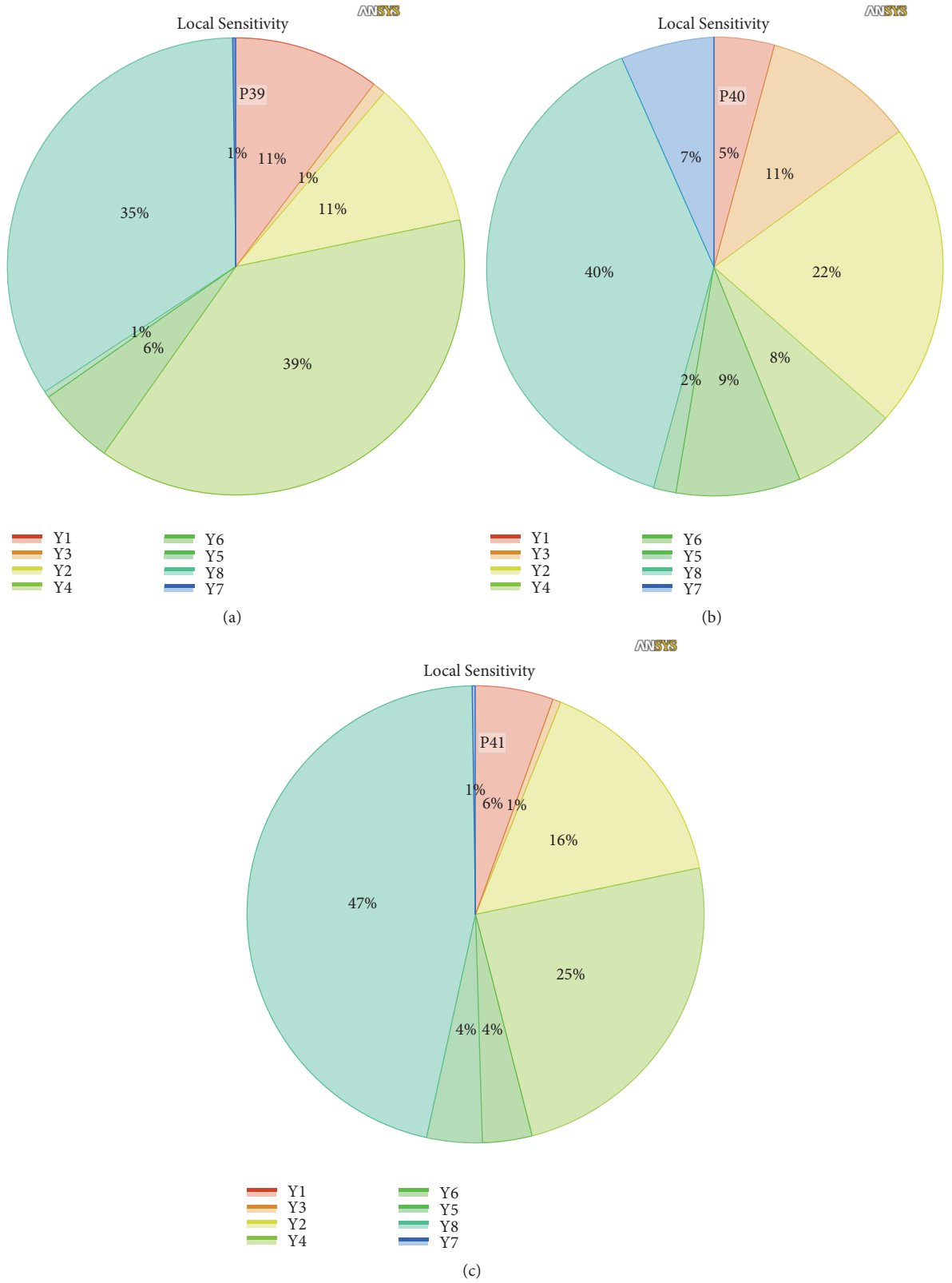

Figure 5: The contributions of overall variables on the dynamic response characteristics, (a) stress response, (b) strain response, and (c) total deformation response.

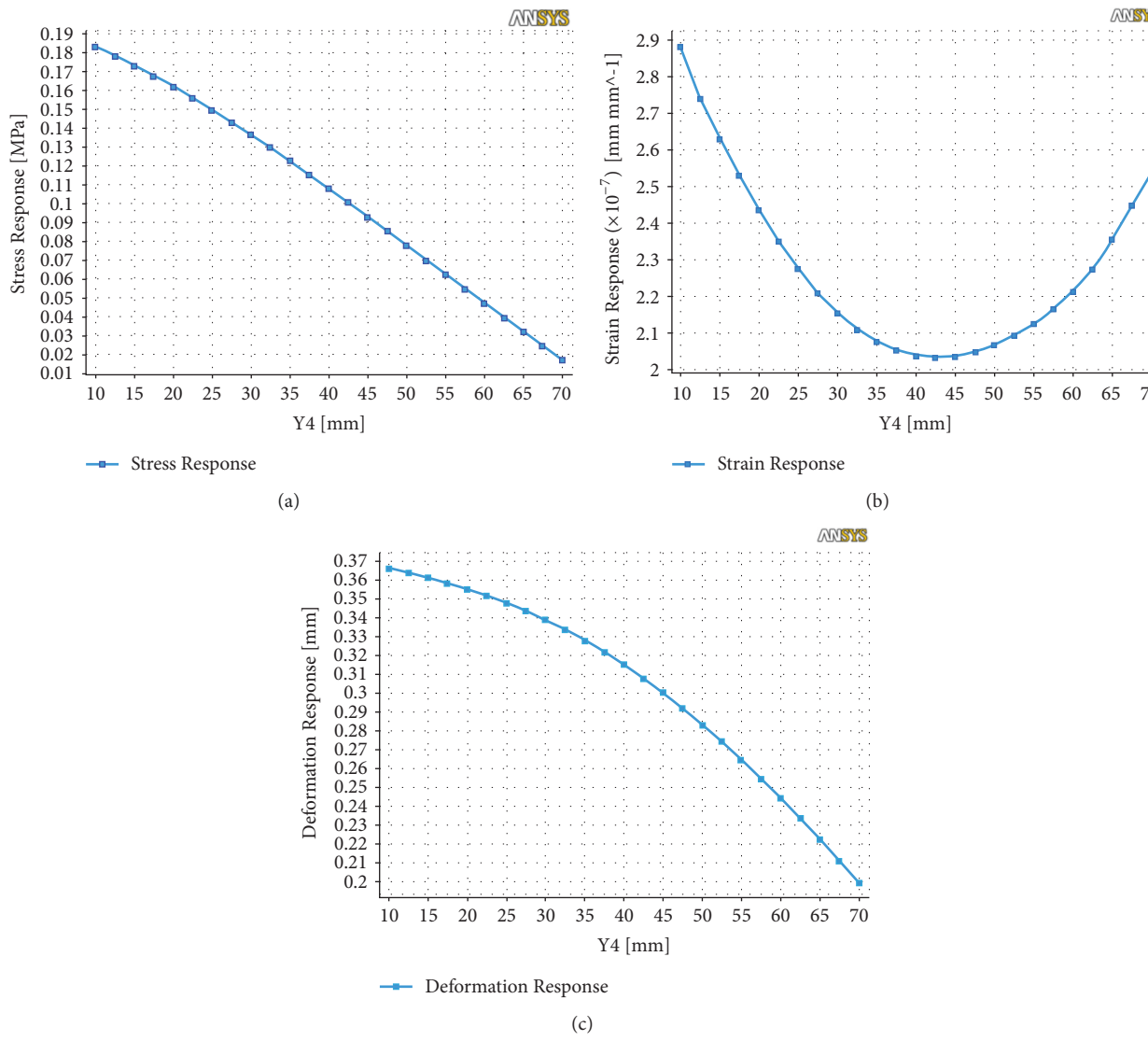

Figure 6: The effect of the distance of the back bearing location on the vibration response characteristics: (a) stress response; (b) strain response; (c) deformation response.

Table 4: The validation experiment for dimensionless amplitude response of MMS.

Item	RS- Evaluation	DO-Real Solution	Ref. [26]	Ref. [27]	Ref. [1]
Dimensionless Amplitude	0.62	0.38	0.43	0.63	0.76

guide for improving the vibration of unbalance response for MMS.

4. Conclusion

In this study, the RS method and forced rotordynamic analyses along with FEA are used to determine the optimal combinations of factors that improve the vibration response characteristics. The spindle specification, bearings locations, cutting force, and motor-rotor unbalance mass are proposed to represent the design factors and then they are utilized to develop MMS. The most popular RS designs of CCDs and BBD methods are used to build the RS models. To visualize more visible variables affecting the dynamic behaviors, the sensitivities analyses and optimization of these variables have been carried out based on RS models. Finally, the quality of RS optimization has been verified by utilizing a direct real solution of the FEM, as well as literature results. The simulation results concluded the following:

(1) A comparison between CCDs and BBD has demonstrated that the BBD is more efficient than the CCDs from the view of RS quality models.

(2) The motor-rotor shaft inner diameter Y2, the distance of back bearing location Y4, and rotating unbalance

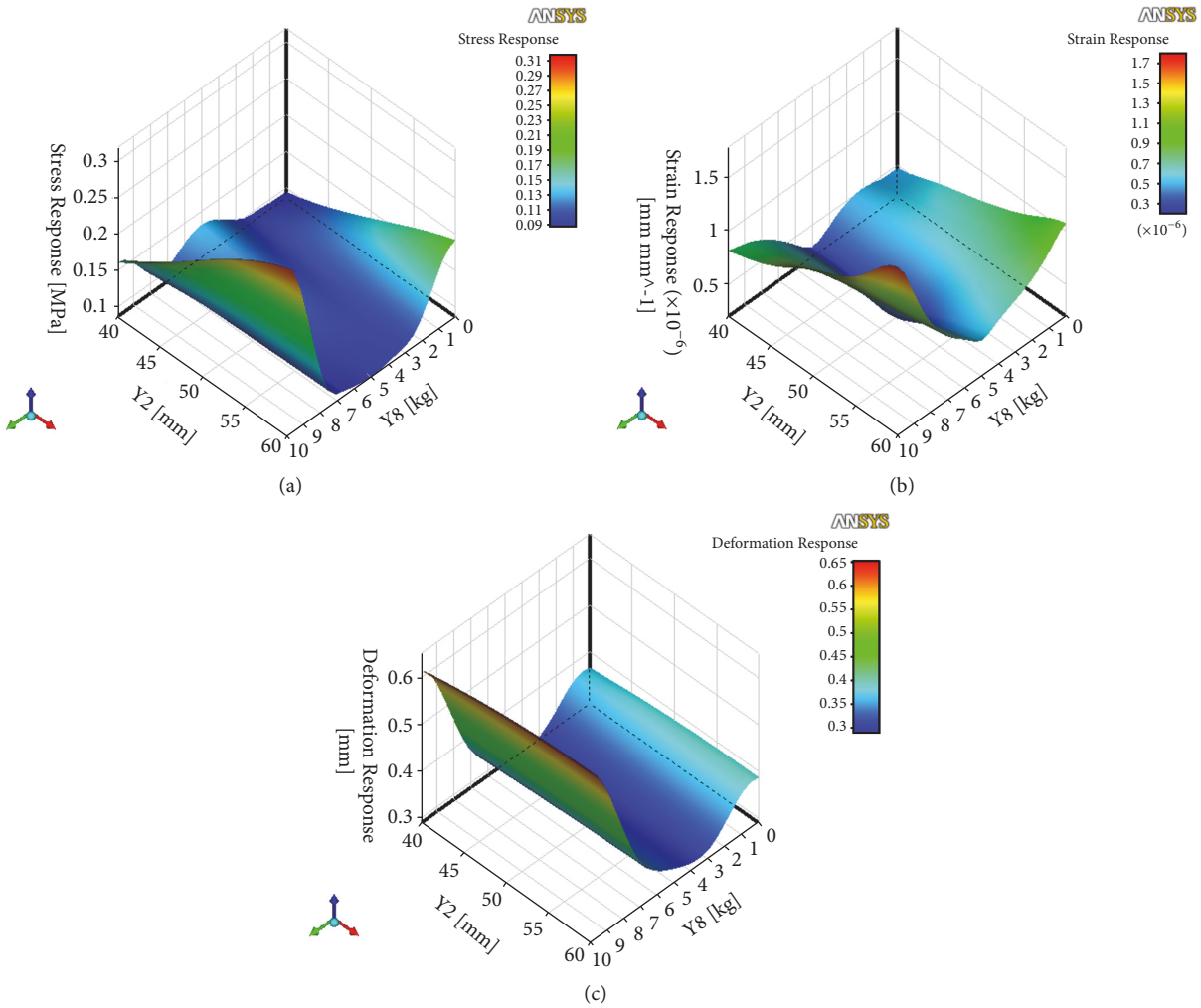

Figure 7: The effect of motor-rotor shaft inner diameter and rotating unbalance mass induced on the vibration response characteristics: (a) stress response; (b) strain response; (c) deformation response.

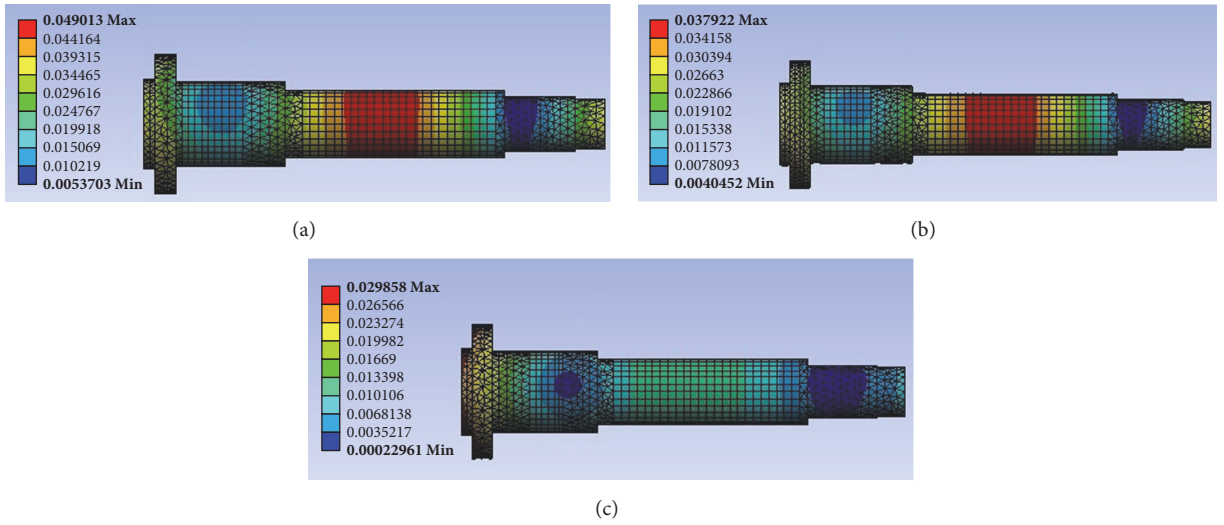

Figure 8: The dynamic TD response after optimization: (a) MOGA; (b) SM for RS; and (c) SM for DO.

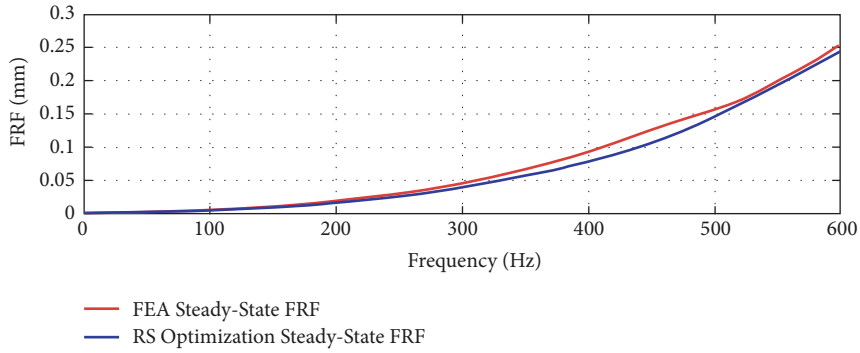

Figure 9: The comparison between the FEA and RS analysis results.

mass Y8 have the greatest effects on the dynamic of unbalance response compared with the other factors.

(3) It is found that more than two-fifths of total vibration response is conducted due to motor-rotor unbalance force induced.

(4) From the view of the verification results, the factors optimization method is practicable and effective in improving the vibration responses characteristics.

Data Availability

The numerical simulation data files used to support the findings of this study are available from the corresponding author upon request.

Conflicts of Interest

The authors declare that there are no conflicts of interest regarding the publication of this paper.

Acknowledgments

This work was supported by the College of Mechanical and Electrical Engineering, Northeast Forestry University, Harbin 150040, China, and the grant fund will be under the responsibility of the corresponding author "Li Shusen". The authors also gratefully acknowledge the technical support provided by it, during conducting this work.

References

[1] P. Huang, W. B. Lee, and C. Y. Chan, "Investigation of the effects of spindle unbalance induced error motion on machining accuracy in ultra-precision diamond turning," *The International Journal of Machine Tools and Manufacture*, vol. 94, pp. 48–56, 2015.

[2] L. B. Kong, C. F. Cheung, S. To et al., "A kinematics and experimental analysis of form error compensation in ultra-precision machining," *The International Journal of Machine Tools and Manufacture*, vol. 48, no. 12-13, pp. 1408–1419, 2008.

[3] S. J. Zhang, S. To, S. J. Wang et al., "A review of surface roughness generation in ultra-precision machining," *The International Journal of Machine Tools and Manufacture*, vol. 91, pp. 76–95, 2015.

[4] M. Habibi, B. Arezoo, and M. Vahebi Nojedeh, "Tool deflection and geometrical error compensation by tool path modification," *The International Journal of Machine Tools and Manufacture*, vol. 51, no. 6, pp. 439–449, 2011.

[5] J. Xul, X. Zheng, J. Zhang et al., "Vibration characteristics of unbalance response for motorized spindle system," *Procedia Engineering*, vol. 174, pp. 331–340, 2017.

[6] S. Jiang and S. Zheng, "Dynamic design of a high-speed motorized spindle-bearing system," *Journal of Mechanical Design*, vol. 132, no. 3, article no. 034501, 5 pages, 2010.

[7] H. Q. Li and Y. C. Shin, "Analysis of bearing configuration effects on high speed spindles using an integrated dynamic thermo-mechanical spindle model," *The International Journal of Machine Tools and Manufacture*, vol. 44, no. 4, pp. 347–364, 2004.

[8] C.-W. Lin and J. F. Tu, "Model-based design of motorized spindle systems to improve dynamic performance at high speeds," *Journal of Manufacturing Processes*, vol. 9, no. 2, pp. 94–108, 2007.

[9] J. Liu and X. Chen, "Dynamic design for motorized spindles based on an integrated model," *The International Journal of Advanced Manufacturing Technology*, vol. 71, no. 9-12, pp. 1961–1974, 2014.

[10] S. Park, C. Lee, and Y. Hwang, "Lightweight design of 45 000 r/min spindle using full factorial design and extreme vertices design methods," *Journal of Central South University of Technology*, vol. 18, no. 1, pp. 153–158, 2011.

[11] C. Lin, "Optimization of bearing locations for maximizing first mode natural frequency of motorized spindle-bearing systems using a genetic algorithm," *Applied Mathematics*, vol. 05, no. 14, pp. 2137–2152, 2014.

[12] Y. Dong, Z. Zhou, and M. Liu, "Bearing preload optimization for machine tool spindle by the influencing multiple parameters on the bearing performance," *Advances in Mechanical Engineering*, vol. 9, no. 2, pp. 1–9, 2017.

[13] I. Asiltürk, S. Neşeli, and M. A. Ince, "Optimisation of parameters affecting surface roughness of Co28Cr6Mo medical material during CNC lathe machining by using the Taguchi and RSM methods," *Measurement*, vol. 78, pp. 120–128, 2016.

[14] D. B. Rao, K. V. Rao, and A. G. Krishna, "A hybrid approach to multi response optimization of micro milling process parameters using Taguchi method based graph theory and matrix approach (GTMA) and utility concept," *Measurement*, vol. 120, pp. 43–51, 2018.

[15] P.-C. Chen, R.-H. Zhang, Y. Aue-u-lan et al., "Micromachining microchannels on cyclic olefin copolymer (COC) substrates with the taguchi method," *Micromachines*, vol. 8, no. 9, p. 264, 2017.

[16] K. Gok, A. Gok, and Y. Kisioglu, "Optimization of processing parameters of a developed new driller system for orthopedic surgery applications using Taguchi method," *The International Journal of Advanced Manufacturing Technology*, vol. 76, no. 5-8, pp. 1437–1448, 2014.

[17] E. Kuram and B. Ozcelik, "Micro-milling performance of AISI 304 stainless steel using Taguchi method and fuzzy logic modelling," *Journal of Intelligent Manufacturing*, vol. 27, no. 4, pp. 817–830, 2016.

[18] H. Mao, L. Jiao, S. Gao et al., "Surface quality evaluation in meso-scale end-milling operation based on fractal theory and the Taguchi method," *The International Journal of Advanced Manufacturing Technology*, vol. 91, no. 1-4, pp. 657–665, 2017.

[19] J. Yang, J. Guan, X. Ye et al., "Effects of geometric and spindle errors on the quality of end turning surface," *Journal of Zhejiang University-SCIENCE A*, vol. 16, no. 5, pp. 371–386, 2015.

[20] D.-S. Lee and D.-H. Choi, "Reduced weight design of a flexible rotor with ball bearing stiffness characteristics varying with rotational speed and load," *Journal of Vibration and Acoustics*, vol. 122, no. 3, pp. 203–208, 2000.

[21] Y.-H. Lin and S.-C. Lin, "Optimal weight design of rotor systems with oil-film bearings subjected to frequency constraints," *Finite Elements in Analysis and Design*, vol. 37, no. 10, pp. 777–798, 2001.

[22] C.-W. Lin, "Simultaneous optimal design of parameters and tolerance of bearing locations for high-speed machine tools using a genetic algorithm and Monte Carlo simulation method," *International Journal of Precision Engineering and Manufacturing*, vol. 13, no. 11, pp. 1983–1988, 2012.

[23] C.-W. Lin, "An application of Taguchi method on the high-speed motorized spindle system design," *Proceedings of the Institution of Mechanical Engineers, Part C: Journal of Mechanical Engineering Science*, vol. 225, no. 9, pp. 2198–2205, 2011.

[24] A. Kutlu, *Design and Development of a Lathe Spindle [M.Sc. Thesis]*, KTH Industrial Engineering and Management, Machine Design, 2016.

[25] A. Labdi and M. Bouchetara, "Optimization of the thermal and mechanical behavior of an aeronautical brake disc using the design of experiments approach," *Mechanics*, vol. 24, no. 2, 2018.

[26] D. Liu, H. Zhang, Z. Tao et al., "Finite element analysis of high-speed motorized spindle based on ANSYS," *The Open Mechanical Engineering Journal*, vol. 5, no. 1, pp. 1–10, 2011.

[27] E. A. I. Ahmed and L. Shusen, "The vibration of machine motorized spindle based on forced rotordynamic analysis and response-surface method," *Vibroengineering PROCEDIA*, vol. 21, pp. 1–7, 2018.

[28] P. H. Joshi, *Machine Tools Handbook*, Tata McGraw-Hill Publishing Company Limited, New Delhi, India, 2007.